JOURNAL OF ATMOSPHERIC AND OCEANIC TECHNOLOGY

Turbulence measurements from velocimeters on compliant mid-water moorings, part 2: motion correction

LEVI KILCHER*, JIM THOMSON, SAMUEL HARDING AND SVEN NYLUND

ABSTRACT

THE ABSTRACT.

1. Introduction

- Brief history of ADVs
- Discussion of ADV v. ADP measurement
- ADVs have been difficult to deploy at mid-depths
- Availability of cheap+accurate IMUs (from smartphone tech) facilitates a new era of ADV measurement from moored platforms.
- Emphasize noise issue and spatial smearing of ADPs.
- Reference to 'Part 1'.
- This work developed for MHK, but has wider applications.

2. Measurements

This work is focused on measuring turbulence from moored ADVs that are equipped with inertial motion sensors (IMU). The ADVs utilized for these measurements were all equipped with Microstrain 3DM-GX3-25 IMU sensors that captured all 6 components of the ADV motion (3 components of angular rotation and 3 components of linear acceleration), as well the orientation of the ADV pressure-case. The sampling of the motion sensor is tightly synchronized with the ADV measurements. The IMU measures its motion at 1kHz and uses internal signal integration (Kalman filtering) to output the motion signals at the same sample rate as the ADV's velocity measurements. This reduces aliasing of the IMU's motion measurements above the ADV's sample-rate (MicroStrain 2010).

*Corresponding author address: National Renewable Energy Laboratory, Golden, Colorado
E-mail: Levi.Kilcher@nrel.gov

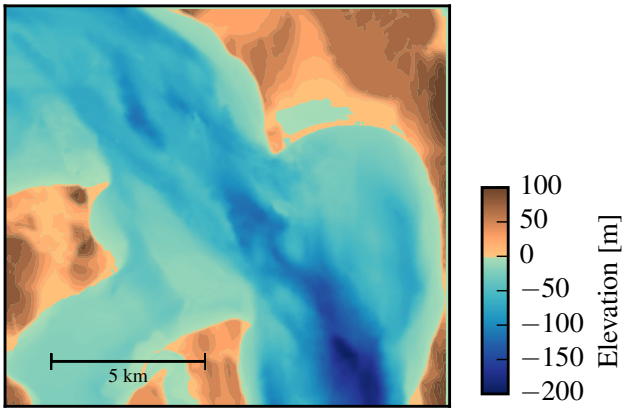

FIG. 1. Bathymetry of Admiralty Inlet at Admiralty Head.

a. Measurements

This work utilizes data from two distinct mooring systems to demonstrate the advantages and limitations of each platform. Both mooring systems were deployed in Admiralty Inlet, Washington, approximately 500 meters (m) WSW of Admiralty Head–Fort Casey State Park–in 60 m of water depth at latitude 48.153 north and longitude 122.687 west (Figure 1). The site is approximately 6 kilometers (km) east of Port Townsend, and 1 km north of the Port Townsend – Coupeville ferry route. Admiralty inlet is the largest waterway connecting Puget Sound to the Strait of Juan de Fuca, and it possesses a large semi-diurnal tidal flow.

1) TIDAL TURBULENCE MOORING (TTM)

The 'Tidal Turbulence Mooring' (TTM) is a simple mooring system with a 'strongback fin' suspended between a steel clump-weight anchor weighing 1200 kilograms (kg, dry) and a 0.93 m-diameter spherical steel buoy with a buoyancy of 320 kg . The ADV pressure cases were

clamped to one side of a 'strongback' fin and the ADV sensor head was positioned 10cm in front of the fin's leading edge (Figure 2). The leading edge of the fin is fastened inline with the mooring line. This configuration was designed to work similar to a weather-vane, such that the drag on the fin held the ADV head upstream of the mooring components. This work utilizes data from two TTM deployments.

The first was in June of 2012 at 48.15285 north, 122.68581 west, near Admiralty Head in Puget Sound, Washington (USA). The mooring was in the water from 17:30 on the 12th until 14:30 on the 14th (local time). Two Nortek ADVs were clamped to either side of the fin such that the axis of their cylindrical pressure-cases were parallel with the leading edge of the strongback. Only one of these ADVs was equipped with an integrated IMU. This TTM also had an upward-looking acoustic Doppler profiler mounted on the mooring anchor.

Periods of time during which this mooring interfered with a beam of the Doppler profiler were identified by inspection of the profiler's acoustic amplitude signal. Periods during which one beam of the profiler had $> 5\%$ higher acoustic amplitude than the other beams were flagged as 'contaminated' and excluded from averaging. 5-minute averages in which more than 50% of the data was contaminated in this way are not shown.

The second TTM deployment was in 2014 from 06:00 on June 17 to 05:00 on June 19. The mooring was positioned at 48.15327 north, 122.68654 west. Two Nortek ADV-IMUs were mounted on this TTM. In this case the pressure-cases and ADV heads were inclined at an angle of 18° to the leading edge of the fin to account for mooring blow-down during strong currents (Figure 3). This change reduced vibrational motion believed to be associated with vortex shedding from the ADV pressure cases when they are oriented cross-wise to the flow (as in the June 2012 deployment).

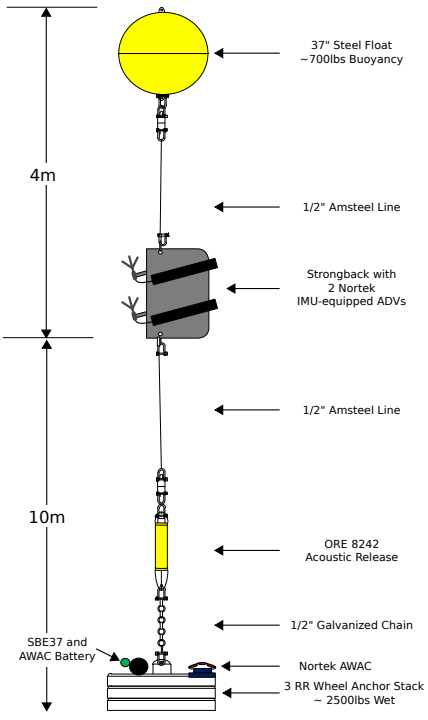

FIG. 2. Schematic diagram of the TTM, not to scale.

FIG. 3. TTM components on the deck of the R/V Jack Robertson. The TTM includes two ADVs, with pressure-cases mounted on opposite sides of the fin. The anchor stack includes a pop-up buoy for retrieval.

2) STABLEMOOR

The second mooring system was a cylindrical syntactic foam buoy (manufacturer: Deep Water Buoyancy) that was anchored to a clump weight that weighed 2700 lbs (Figure 4). The buoy is 3.5 m long and 0.45 m in diameter with a tail ring that is 0.76 m in diameter. The buoy was deployed from 11:21 on May 11, 2016 to 12:00 on May 12, 2016 at 48.15277 north, 122.68623 west.

The StableMoor platform has two primary advantages compared to the TTM. First, it is significantly more massive and hydro-dynamically stable than the TTM, which reduces the frequency of motions of the platform. The other major advantage of the StableMoor platform is that it is capable of supporting an acoustic Doppler profiler that provides an independent measure of the platform's translational motion by bottom-tracking. The disadvantages of the Stable Moor is that its size introduces new challenges in deployment and recovery, and it is significantly more expensive than the TTM system.

The StableMoor weighs 295 kg in air, and has a buoyancy of 185 kg in water. An ADV head was positioned 0.1 m in front of the buoy nose. The buoy was equipped with a 1200 kHz RDI workhorse sentinel acoustic Doppler profiler that was pointed downward and configured to measure water velocity below the platform in 12 1-meter bins and measure buoy motion ('bottom tracking'), all at a 1 Hz

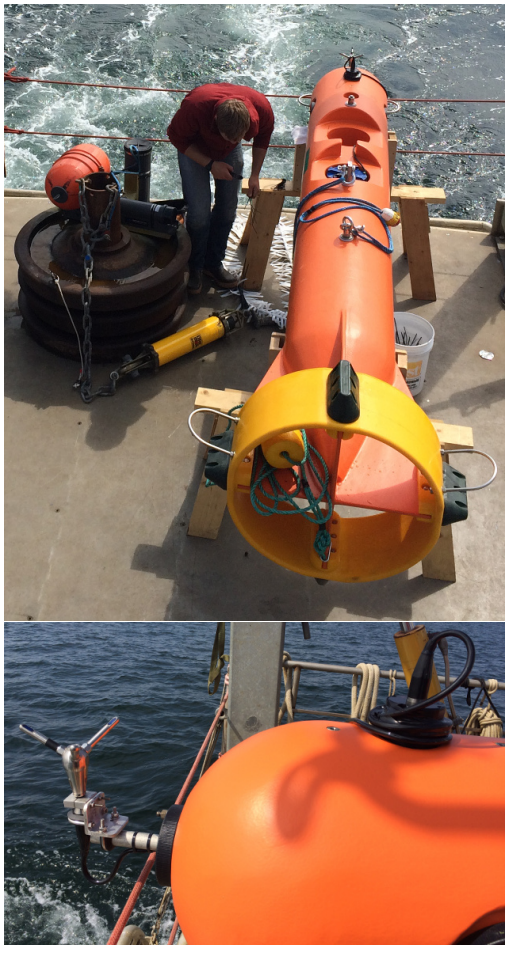

FIG. 4. Alex DeKlerk checks to ensure that the StableMoor buoy is properly fastened to its anchor; the RDI workhorse ADCP can be seen in the rear instrument bay (top). A bridle is draped across the top of the buoy for deployment and recovery, and a small marker buoy fastened to the tail is useful during recovery. A close-up of the StableMoor nose shows the ADV head and the top of its pressure case (bottom).

sample rate. The bottom track velocity provides an independent measure of platform motion that aids in correcting velocity measurements for mooring motion.

The buoy platform was ballasted to pitch upward a few degrees in zero-flow to avoid 'flying downward'. In the presence of an oncoming current the tail fins help to orient it into the flow. The anchor for this buoy is similar to that of the TTM, including an acoustic release so the mooring and anchor can be recovered separately. Additional details, photos, and schematic diagrams of both mooring systems are available in Harding et al. (2016).

b. Principal-axes coordinate system and turbulence averaging

Unless stated otherwise, vector quantities in this work are in a fixed 'principal-axes' coordinate system that is aligned with the bi-directional tidal flow: positive u is in the direction of ebb (310° True), positive w is vertically upward, and v is the cross-stream component in a right-handed coordinate system. The full velocity vector, $\vec{\tilde{u}} = (\tilde{u}, \tilde{v}, \tilde{w})$, is separated into a mean and turbulent component as $\vec{\tilde{u}} = \vec{\bar{u}} + \vec{u}$, where the over-bar denotes a 5 minute average. Turbulence kinetic energy, tke $= \overline{u^2} + \overline{v^2} + \overline{w^2}$, and Reynold's stresses, $\overline{uv}$, $\overline{uw}$, $\overline{vw}$ are computed by averaging over the 5-minute window. Throughout this work we use $\bar{U} = (\bar{u}^2 + \bar{v}^2)^{1/2}$ to denote the horizontal velocity magnitude.

All spectra, $S\{x\}(f) = |\mathscr{F}\{x(t)\}|^2$, and cross-spectra, $C\{x,y\}(f) = \text{real}(\mathscr{F}\{x(t)\}\mathscr{F}\{y(t)\})$, are computed using NumPY fast Fourier transform routines (van der Walt et al. 2011). Here, $\mathscr{F}\{x(t)\}$ denotes the fast Fourier transform of a signal $x(t)$. Time series' are linearly detrended and Hanning windowed prior to computing $\mathscr{F}\{\{\}x\}$ to reduce spectral reddening. Throughout the remainder of this work the dependence of S and C on f is implied (e.g. $S\{x\}(f)$ is hereafter $S\{x\}$), and all other variables are functions of t. Spectra and cross-spectra are normalized to preserve variance: $\int S\{u\}\mathrm{d}f = \overline{u^2}$, and $\int C\{u,v\}\mathrm{d}f = \overline{uv}$. The notations $S\{\vec{u}\} = (S\{u\}, S\{v\}, S\{w\})$ and $C\{\vec{u}\} = (C\{u,v\}, C\{u,w\}, C\{v,w\})$ denote the set of spectra and cross-spectra for each velocity component and pairs of components, respectively.

Turbulence dissipation rates are computed as,

$$\varepsilon = \frac{1}{\bar{U}} \left(\alpha \left\langle (S\{u\} + S\{v\} + S\{w\}) f^{5/3} \right\rangle_{fIS} \right)^{3/2} \qquad (1)$$

Where $\alpha = 0.5$, and $\langle\rangle_{fIS}$ denotes an average over the inertial-subrange of the velocity spectra and where the signal-to-noise ratio is small (Lumley and Terray 1983; Sreenivasan 1995). Throughout this work we take this average from 0.3 to 1 Hz for the u and v components, and 0.3 to 3 Hz for the w component.

3. Methodology

The essential approach of this methodology is to estimate time-series of velocity on a compliant mooring by obtaining an independent estimate of ADV head motion and removing that motion from the measured signal. Nortek offers an ADV that is equipped with an IMU that measures the linear acceleration, rotational-motion, and orientation of the ADV pressure case (body). So long as the ADV head is rigidly connected to the ADV pressure case, it is possible to utilize the IMU motion signals to calculate the motion of the ADV head, and remove it from the measured velocity signal. The ADV head motion, is calculated as the sum of rotational and translational motion, which are each estimated from the IMU's angular-rate, $\vec{\omega}$,

and acceleration, $\vec{a}$, signals as:

$$\vec{u}_{\rm h} = \vec{u}_\omega + \vec{u}_a + \vec{u}_{\rm low} \quad (2)$$

$$= \mathbf{R}^{\rm T} \cdot \vec{\omega}^*(t) \times \vec{\ell}^* + \int \{\vec{a}(t)\}_{HP(f_a)} {\rm d}t + \vec{u}_{\rm low} \quad (3)$$

Here '$*$' superscripts denote quantities in the ADV's locale coordinate system, $\mathbf{R}^{\rm T}$ is the IMU orientation matrix that rotates vectors from the IMU to the earth reference frame, and $\vec{\ell}^*$ is the vector from the IMU to the ADV head. The notation $\{\vec{a}\}_{HP(f_a)}$ indicates that the IMU's accelerometer signal is high-pass filtered (in the earth's stationary reference frame) at a chosen filter-frequency, f_a. This is necessary because accelerometers have low-frequency noise, sometimes referred to as 'bias-drift' (Barshan and Durrant-Whyte 1995; Bevly 2004; Gulmammadov 2009). Bench-tests of the Microstrain IMU indicate that its accelerometers drift for frequencies $< 10^{-2}$Hz (Egeland 2014). This noise is amplified by integration of the acceleration signal such that it contaminates the motion correction, especially at low-frequencies (Figure 3). This issue means that low-frequency motion is not well resolved by the IMU, and so there is a residual low-frequency translational motion, $\vec{u}_{\rm low}$, that needs to be considered when performing motion correction.

The choice of high-pass filter to be used to correct for low-frequency accelerometer noise issue on the application (e.g. deployment platform), and the turbulence level of the measurement environment. In particular, this involves a trade off between filtering-out this noise and not filtering measured motion that is unresolved by an independent measurement of $\vec{u}_{\rm low}$. If an independent measure of low-frequency motion is available it can be used to increase the accuracy of $\vec{u}_{\rm h}$ at low-frequency. Note that, to avoid double counting, $\vec{u}_{\rm low}$ should be estimated by applying the complimentary low-pass filter to the independent measurement of low-frequency motion.

With this estimate of ADV head motion it is straightforward to correct the measured velocity, $\vec{u}_{\rm m}$, to estimate the velocity in the earth's inertial reference frame:

$$\vec{u}(t) = \vec{u}_{\rm m}(t) + \vec{u}_{\rm h}(t) \quad . \quad (4)$$

Note here that the '+'-sign is correct because head motion, $\vec{u}_{\rm h}$, induces a measured velocity in the opposite direction of the head motion itself ($\vec{u}_{\rm m} = \vec{u} - \vec{u}_{\rm h}$).

For the TTM and Turbulence Torpedo we utilize $f_a = 0.0333Hz$ (30 second period), and assume that $\vec{u}_{\rm low} = 0$. For the StableMoor $f_a = 0.2Hz$ (5 second period). The bottom-track velocity was low-pass filtered at this frequency to provide an estimate of $\vec{u}_{\rm low}$, and $\vec{a}$ was high-pass filtered at this frequency. We use 4-pole, bi-directional (zero-phase), Hanning filters for all filtering operations.

Additional details on motion correction–including a detailed accounting of the distinct coordinate systems of the IMU, ADV pressure case, and ADV head–can be found in Kilcher et al. (2016). Open-source Python tools for performing motion correction of ADV-IMU data–including scripts that write processed data in Matlab and tabulated formats–are available at `http://lkilcher.github.io/dolfyn/`.

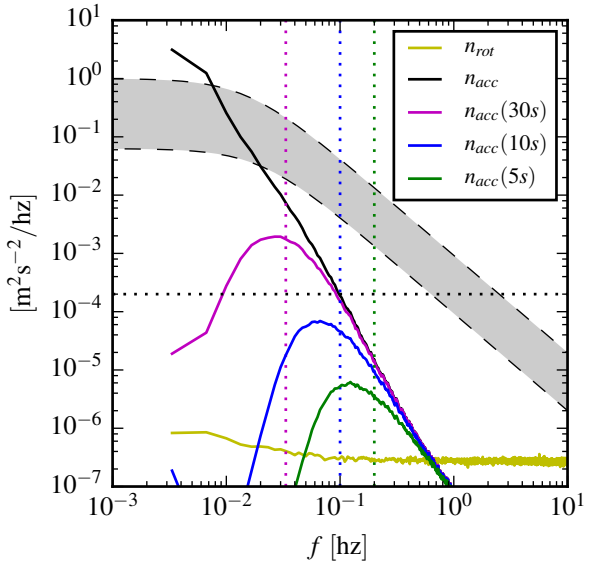

FIG. 5. Spectra of $\vec{u}_\omega$ (yellow) and $\vec{u}_a$ signals from the Microstrain IMU sitting on a motionless table. The $\vec{u}_a$ signals are unfiltered (black), and high-pass filtered at 30s (magenta), 10s (blue), 5s (green). Vertical dotted lines indicate the filter frequency. The black horizontal dotted line indicates the noise-level of a Nortek Vector ADV configured to measure $\pm$4m/s. The shaded region indicates the range of spectra presented herein (0.002 < tke < 0.03 $\mathrm{m^2/s^2}$, 1e-5 < ε < 5e-4 W/kg).

4. Results

a. Mean velocity

A comparison of mean velocity measured by an ADV-IMU mounted on a TTM, to that of an upward-looking acoustic Doppler profiler mounted on the TTM anchor is presented in Figure 6. This shows excellent agreement between the ADV and Doppler profiler measurements of velocity. The u, v and w components have a root-mean-square error of 0.05, 0.13 and 0.03 m/s, respectively. While it is important to note that their is some discrepancy between ADP and ADV measured velocities (especially in the v-component, which is most likely due to incomplete motion correction), the agreement between the magnitude and direction of these independent velocity measurements indicates that moored ADV-IMUs provide a reliable estimate of velocity in the Earth's reference frame.

b. TTM Spectra

As discussed in detail in Part 1 the mooring motion of the TTM, $S\{\vec{u}_{\rm h}\}$, has a peak at 0.1 to 0.2 Hz from swaying

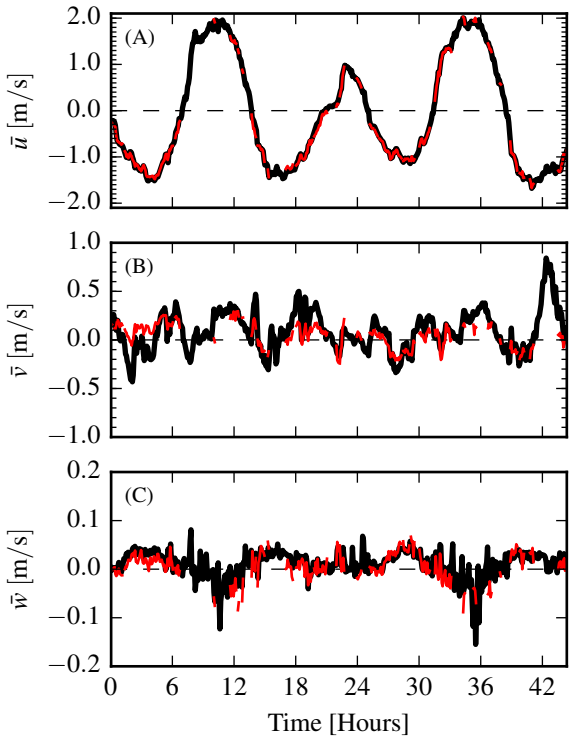

FIG. 6. Time series of tidal velocity at Admiralty Head from TTM measurements (black), and an acoustic Doppler profiler (red). The profiler measurements–taken at the same depth as the ADV on the TTM—were contaminated by acoustic reflection from the strongback fin when it was inline with one of the profiler's beams. Note that the vertical scale on the three axes vary by more than an order of magnitude; the small ticks in A and B are equivalent to the ticks in C.

of the mooring that is most likely driven by eddy-shedding from the spherical buoy (Figure 7, red lines). There is also broad-band motion that is associated with fluttering of the strongback fin around the mooring line. Both of these motions are especially energetic in the v-component spectra, because this is the direction in-which the TTM mooring system is most unstable. As is expected from fluid-structure interaction theory the amplitude of these motions increases with increasing mean velocity (Morison et al. 1950).

The mooring motion contaminates the uncorrected ADV-measurements of velocity, $S\{\vec{u}_\mathrm{m}\}$, whenever the amplitude of the motion is similar to or greater than the amplitude of the turbulence. Fortunately, much of this motion can be removed using the IMU's motion signals as detailed in section 3. Lacking an independent measurement of turbulence velocity at this site, we interpret the agreement of these spectra with turbulence theory as evidence of the success of the method. In particular, at high-frequencies ($f > 0.3$ Hz) for each mean-flow speed the spectra decay with a $f^{-5/3}$ slope and have equal amplitude across the velocity components. These results are consistent with Kolmogorov's (1941) theory of isotropic turbulence, and are consistent with other measurements of turbulence in energetic tidal channels from stationary platforms (Kolmogorov 1941; Walter et al. 2011; Thomson et al. 2012; McMillan et al. 2016).

At low frequencies, the spectra tend to become roughly constant (especially at higher flow speeds), which is also consistent with previous works. Note here, that the very-low magnitude of $S\{\vec{u}_\mathrm{h}\}$ at low frequencies is partially a result of filtering the IMU's accelerometer signal when calculating $\vec{u}_a$. The true low-frequency spectrum of ADV-head motion is unknown (indicated using a dashed line below f_a). A comparison of $S\{\vec{u}\}$ measured by the TTM to that measured by the ADP–during the June 2012 deployment–are in agreement at low-frequencies. This suggests that the assumption that $\vec{u}_\mathrm{low} = 0$ at these frequencies, at this site, for this platform is justified–even if $S\{\vec{u}_\mathrm{h}\}$ is not as low as indicated in Figure 7.

As successful as motion correction is, some of the motion contamination persists in $S\{\vec{u}\}$. This is most notable in the v-component spectra at the highest flow speeds where a peak in $S\{v\}$ at 0.15 Hz is nearly an order of magnitude larger than a typical turbulence spectral fit to the other frequencies would indicate. This persistent motion contamination is evident to a lesser degree in the u-component spectra at the highest flow speed, and in the v-component spectra at lower flow speeds. The w-component spectra appear to have no persistent motion contamination. This is largely because the amplitude of the motion in this direction is much lower than for the other two components. In fact, for these measurements, the w-component of mooring motion is so low that w-component motion correction is significant only at the highest flow speeds (i.e. motion correction removes the 0.15 Hz peak).

The amplitude of the persistent motion contamination peaks at 0.15 Hz are a factor of 5 to 10 times smaller than the amplitude of the ADV head motion itself. This suggests the Microstrain IMU can be used to effectively correct for mooring motion at 0.15 Hz when the amplitude of that motion is less than 5 times the amplitude of the real turbulence spectrum.

This reveals an ancillary benefit of the IMU measurements, which is that they can assist with identifying and accounting for persistent sources of motion contamination. For example, one of the most common uses of turbulence spectra is for the calculation of the turbulent kinetic energy dissipation rate, ε, or for calculating the total turbulent kinetic energy, tke. For these purposes, based on the relative amplitudes of the 0.15 Hz peaks, we assume that persistent motion contamination is likely where $S\{\vec{u}_\mathrm{h}\}/S\{\vec{u}\} > 3$ and exclude these regions from spectral fits.

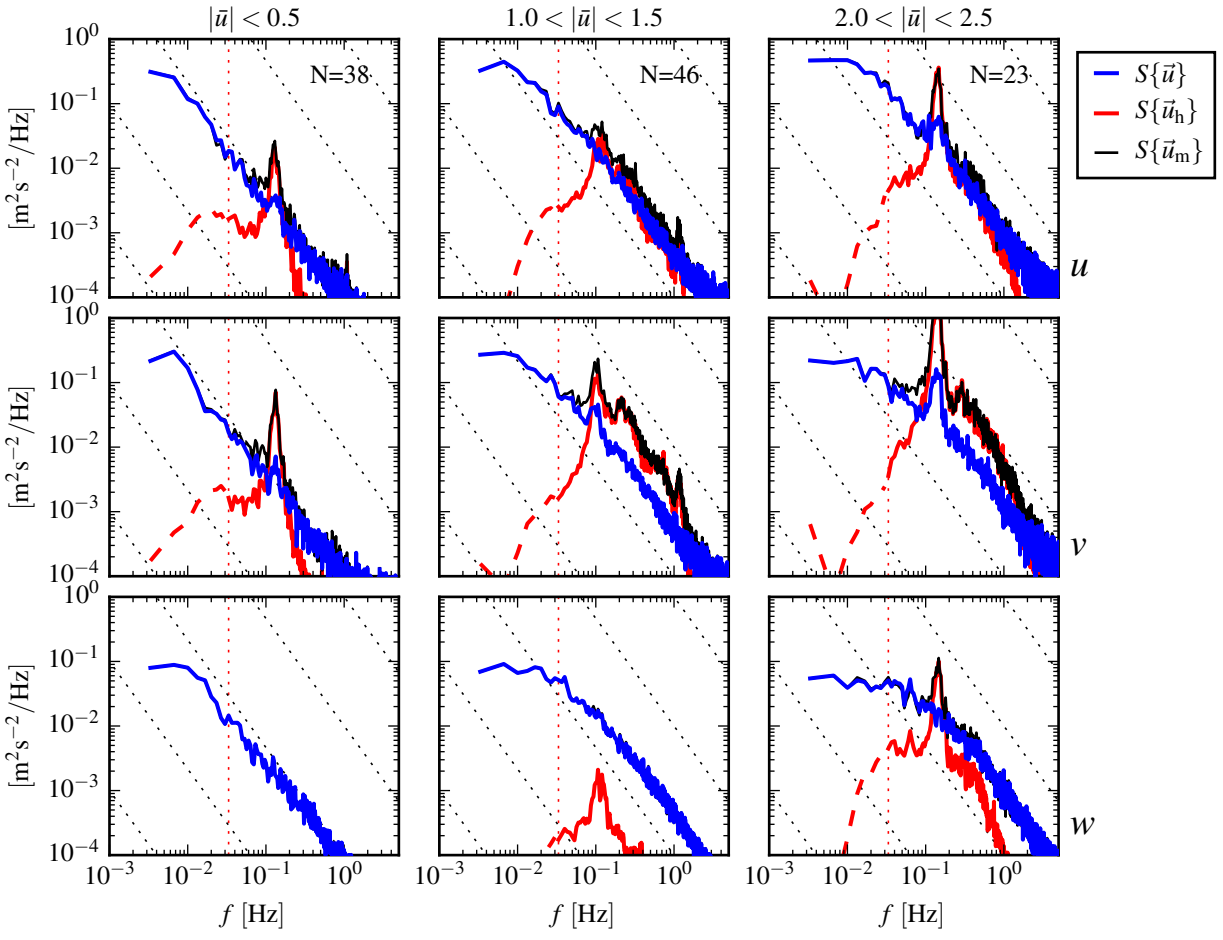

FIG. 7. Turbulence spectra from the June 2014 TTM deployment. Each column is for a range of streamwise velocity magnitudes (indicated at top). The rows are for each component of velocity (indicated to the lower-right of the right column). The uncorrected spectra are in black and the corrected spectra are blue, and the spectra of ADV head motion, $\vec{u}_h$, is red (also indicated in the legend). The vertical red dotted line indicates the filter frequency applied to the IMU accelerometers when estimating $\vec{u}_h$; below this frequency $S\{\vec{u}_h\}$ is plotted as a dashed line. Diagonal black dotted lines indicate a $f^{-5/3}$ slope. The number of spectral-ensembles, N, in each column is indicated in the top row.

In the present case, for the u and w spectra, this criteria only excludes a narrow range of frequencies at the 0.15 Hz motion peak for some cases. This criteria is more restrictive of the v-component spectra at high frequencies for $U > 1.0$ m/s, but this may be acceptable because the amplitude of the spectrum at these frequencies—i.e. in the isotropic inertial subrange—should be equal to that of u and w (Kolmogorov 1941).

Agreement of the v-component spectral amplitude with that of u and w at frequencies > 0.3 Hz indicates that motion correction is effective at those frequencies even when $S\{\vec{u}_h\}/S\{\vec{u}\} > 3$. This suggests that our screening threshold is excessively conservative at those frequencies, and that a more precise screening threshold is frequency dependent. For example, it might take into account the f^3 character of the noise in $S\{\vec{u}_a\}$ (Figure 3). For the purposes of this work the $S\{\vec{u}_h\}/S\{\vec{u}\} < 3$ threshold for spectral fits is sufficient, and detailed characterization of the IMU's motion- and frequency-dependent noise level is left for future work.

c. StableMoor Spectra

The spectra of the stablemoor motion has a broader peak with a maximum amplitude that is at approximately half the frequency of the TTM spectral peak (Figure 8). The motion of this platform also does not have high-frequency 'sub-peaks' or other high-frequency broad-banded excitation. These characteristics of the motion are most-likely due to the more massive and hydrodynamically streamlined nature of the platform.

Like the TTM, the motion-corrected spectra from the StableMoor are consistent with turbulence theory and pre-

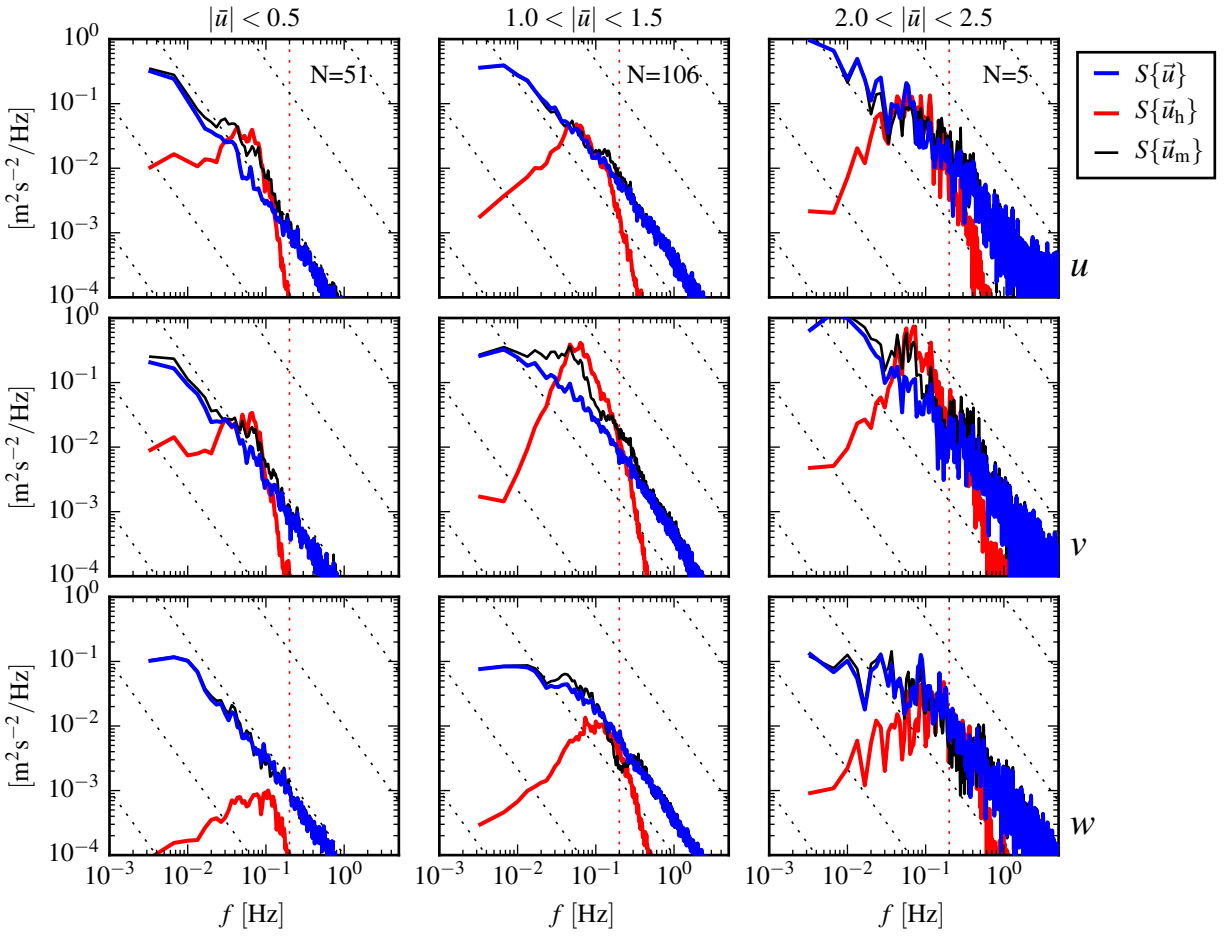

FIG. 8. Turbulence spectra from the StableMoor buoy. The axes-layout and annotations are identical to Figure 7, except that $S\{\vec{u}_h\}$ is plotted as a solid line at all frequencies because it is measured at all frequencies.

vious observations. Most importantly, there is an improvement in the quality of the motion corrected spectra compared to the TTM. In particular the persistent motion contamination peaks are essentially gone. That is, this measurement system provides an accurate estimate of the turbulence spectra at this location from low frequencies to more than 1Hz—well into the inertial sub-range.

Note that this level of accuracy can not be obtained without the independent estimate of $\vec{u}_{low}$. That is, if we assume that $\vec{u}_{low} = 0$ a similar plot to Figure 8 (not shown) reveals persistent motion-contamination peaks and troughs in the u- and v-spectra regardless of the choice of f_a. This indicates that the low-frequency motion of the StableMoor is below a threshold where the IMU's signal to noise ratio is high enough to resolve its motion. In other words, compared to the TTM, the StableMoor platform provides a more accurate measurement of turbulence when it includes an independent measure of $\vec{u}_{low}$ (here a bottom-tracking ADCP), but it does no better—and perhaps worse—when it doesn't.

d. Torpedo Spectra

The u and v motion of the Turbulence Torpedo is broadbanded and the w motion has a narrow peak at 0.3 Hz (Figure 9). Because $\vec{u}_h$ is estimated using $f_a = 0.0333Hz$ and assuming $\vec{u}_{low} = 0$ its spectra rolls-off quickly below f_a. Side note: even with the high-pass filtering the integration of the low-f accelerometer noise appears as a 'rebound' of the spectrum of $\vec{u}_h$ at the lowest frequencies.

Motion correction of the Torpedo data appears to effectively remove a motion from the w-component spectra at 0.3Hz, and straightens out the v-component spectra between 0.04 and 0.6Hz. The u-component motion is relatively unimproved by motion correction, apparently because the Torpedo motion is slightly smaller than the turbulence in this direction. At frequencies below f_a, the spectral amplitude of the u- and v-components increase

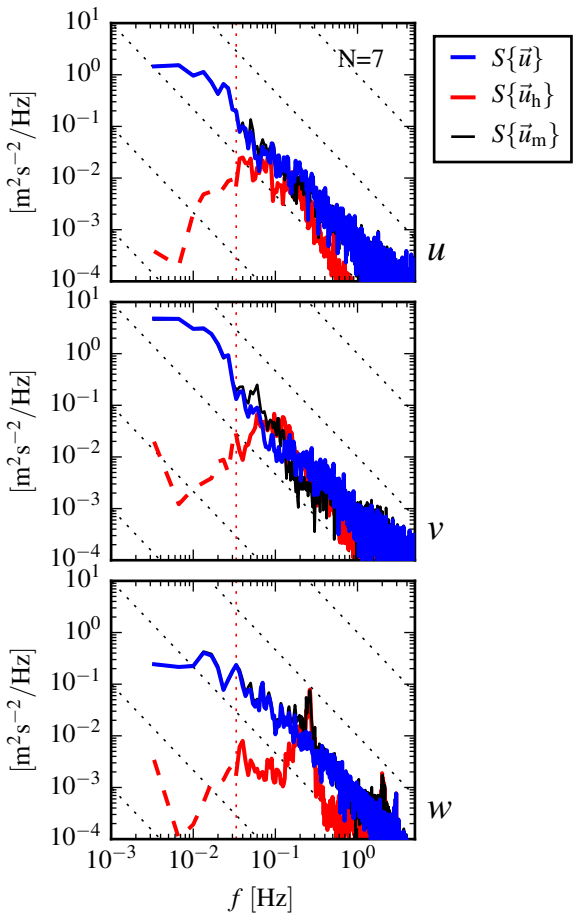

FIG. 9. Turbulence spectra from the turbulence torpedo during a 35 minute period when the mean velocity was 1.3 m/s. Annotations and line colors are identical to Figure 7.

dramatically. This suggests that unresolved low-frequency motion of the Torpedo is contaminating the velocity measurements at these frequencies. It may be possible to correct for some of this using a measurement of the ship's motion as a proxy for the Torpedo's low-frequency motion, but this has not been done. Still, above f_a, the Torpedo appears to provide a reliable estimate of spectral amplitude in the inertial subrange and can therefore be used to estimate ε. Considering the simplicity of the Torpedo it may be a useful option for quantifying this essential turbulence quantity. If a GPS is positioned above it, it may be capable of providing even more.

e. Cross-spectra

Inspection of cross-spectra from TTM measurements demonstrates that motion correction can reduce motion contamination to produce reliable estimates of velocity cross-spectra (Figure 10). At low flow speeds (left column), cross-spectra between components of $\vec{u}_h$ (i.e. between components of head-motion, red) are small compared to correlated velocities. This indicates that there is minimal need for motion correction to estimate cross-spectra and Reynold's stresses. As the velocity magnitude increases (center, and right columns), the swaying motion of the TTM at 0.15 Hz appears as a peak in the amplitude of the cross-spectra of $\vec{u}_h$ and $\vec{u}_m$ (black) for all three components of cross-spectra (rows). Fortunately, motion correction reduces the amplitude of this peak dramatically, so that $C\{\vec{u}\}$ (blue) is small at 0.15 Hz compared to lower frequencies. Furthermore, the fact that the standard deviation of $C\{\vec{u}\}$ is also relatively small at 0.15 Hz suggests that motion correction is effective for each spectral window, not just in their mean.

This result indicates that motion-corrected TTM velocity measurements can be used to obtain reliable estimates of turbulence Reynold's stresses, which are the integral of the cross-spectra. Without motion correction, Reynold's stress estimates would be contaminated by the large peaks in the cross-spectra that are due to the swaying and fluttering motion of the TTM vane.

A similar investigation of StableMoor cross-spectra (not shown) indicates that cross-spectral motion contamination is much lower amplitude than for the TTM. The low-frequency (< 0.3 Hz) 'swimming' motion of that platform produces minimal cross-spectral signal, and the relative large-mass of the platform minimizes the kinds of higher-frequency swaying/fluttering that creates large values of cross-spectral head-motion. Thus, the StableMoor platform also produces reliable estimates of Reynold's stresses, which are presumed to be improved by motion correction.

5. Discussion

The beginning of the previous section presented a comparison of $\vec{u}$ measured by a TTM-mounted ADV, to measurements from a co-located ADP. This demonstrated that the IMU provides a reliable estimate of the ADV's orientation and that this can be utilized to estimate mean velocity in the earth's reference frame. Turbulence velocity estimates from the same ADP are also in agreement with low-frequency TTM turbulence estimates (not shown), but the ADP does not resolve turbulence at the scales where motion contamination is strongest (0.1 to 1.0 Hz).

Ideally, moored motion-corrected turbulence velocity measurements would be validated against simultaneous independent validated measurements of turbulence velocity at the same scales and exact location. Accomplishing this, however, involves significant technical challenges not easily overcome—most notable is the challenge of measuring turbulence at the same point as the moving ADV. A slightly less ideal but much more realistic confirmation

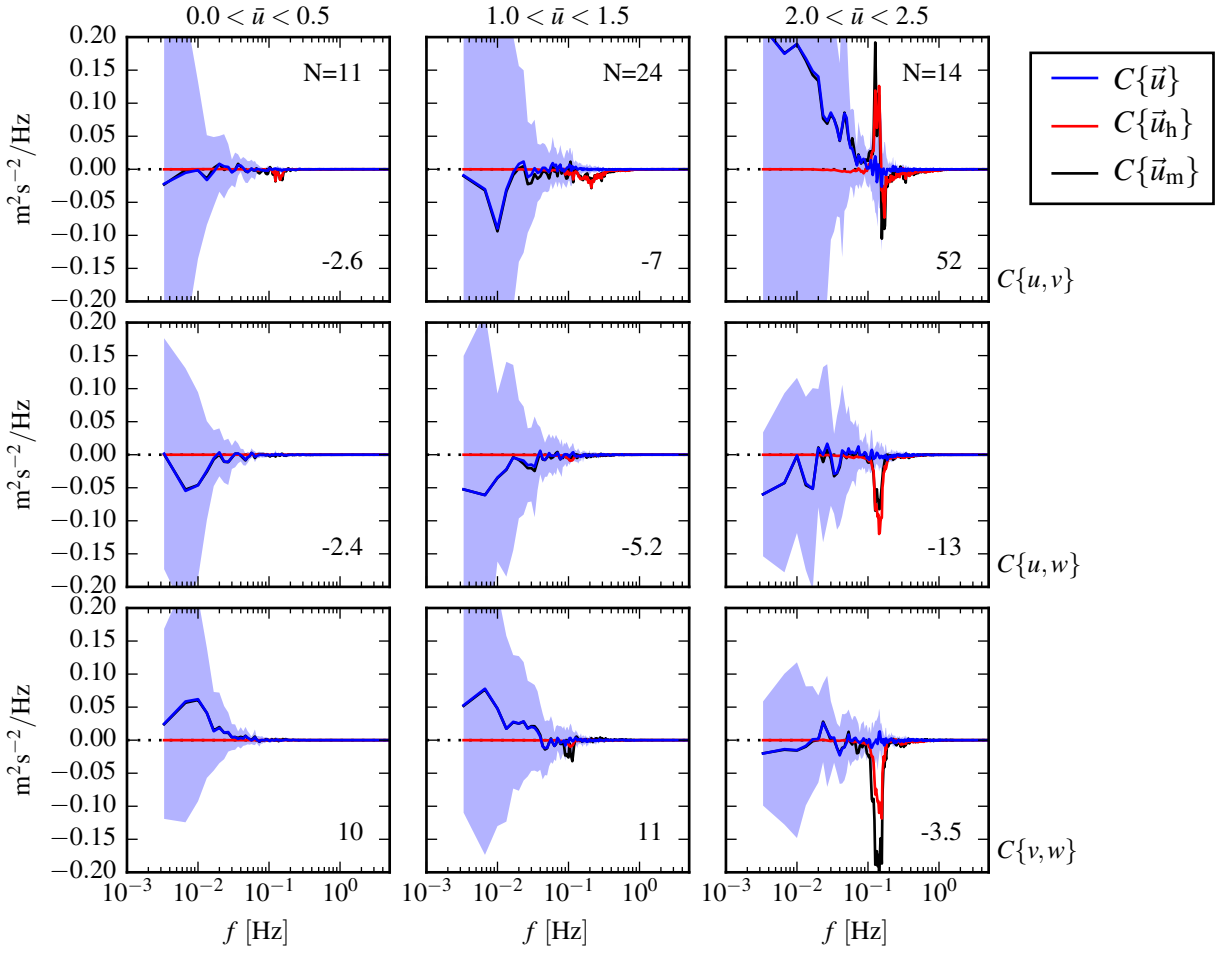

FIG. 10. The real part of the cross-spectral density between velocity components measured by the TTM. The upper-row is the *u*-*v* cross-spectral density, the middle-row is the *u*-*w* cross-spectral density, and the bottom-row is the *v*-*w* cross-spectral density. The columns are for different ranges of the stream-wise mean velocity magnitude (indicated above the top row). The blue line is the cross-spectrum between components of motion-corrected velocity, the red line is the cross-spectrum between components of head-motion, and the black line is the cross-spectrum between components of uncorrected velocity. The light-blue shading indicates one standard deviation of the *C* for the motion corrected cross-spectral density. N is the number of spectral ensembles in each column. The number in the lower right corner of each panel is the motion-corrected Reynold's stress (integral of the blue line) in units of 1e-4 m^2s^{-2}.

of the methodology might involve comparing the statistics of moored turbulence measurements to that from a nearby fixed platform, but such measurements have not yet been made (e.g. the 'TTT' platform described in Thomson et al. 2012).

Lacking an independent stationary turbulence measurement near the moored measurements, it is instructive to demonstrate the degree to which the moored measurements are consistent with turbulence theory and other turbulence measurements in similar flow environments. The previous section showed that the shape of the turbulence velocity spectra from moored ADVs is consistent with Kolmogorov's theory of locally isotropic turbulence, which has been observed consistently in turbulence measurements for decades (Kolmogorov 1941; Grant et al. 1962; McMillan et al. 2016). In particular, we observed an isotropic subrange—an $f^{-5/3}$ spectral slope, and equal amplitude spectra between components—that is driven by anisotropic turbulence at longer time-scales (Figures 7, 8, 9). This is interpreted as the first indication that the measurement systems presented are capable of accurately resolving turbulence. The degree to which uncorrected spectra were corrected toward this theoretical and observationally confirmed shape is interpreted as a measure of the improvement of the spectral estimates by motion correction.

Figure 11 presents a time-series of the mean velocity (A) and several turbulence statistics that have were measured during the June 2014 TTM deployment. This figure shows the evolution of the flow through Admiralty Inlet during 1.5 tidal cycles. The tke (B), Reynold's stresses

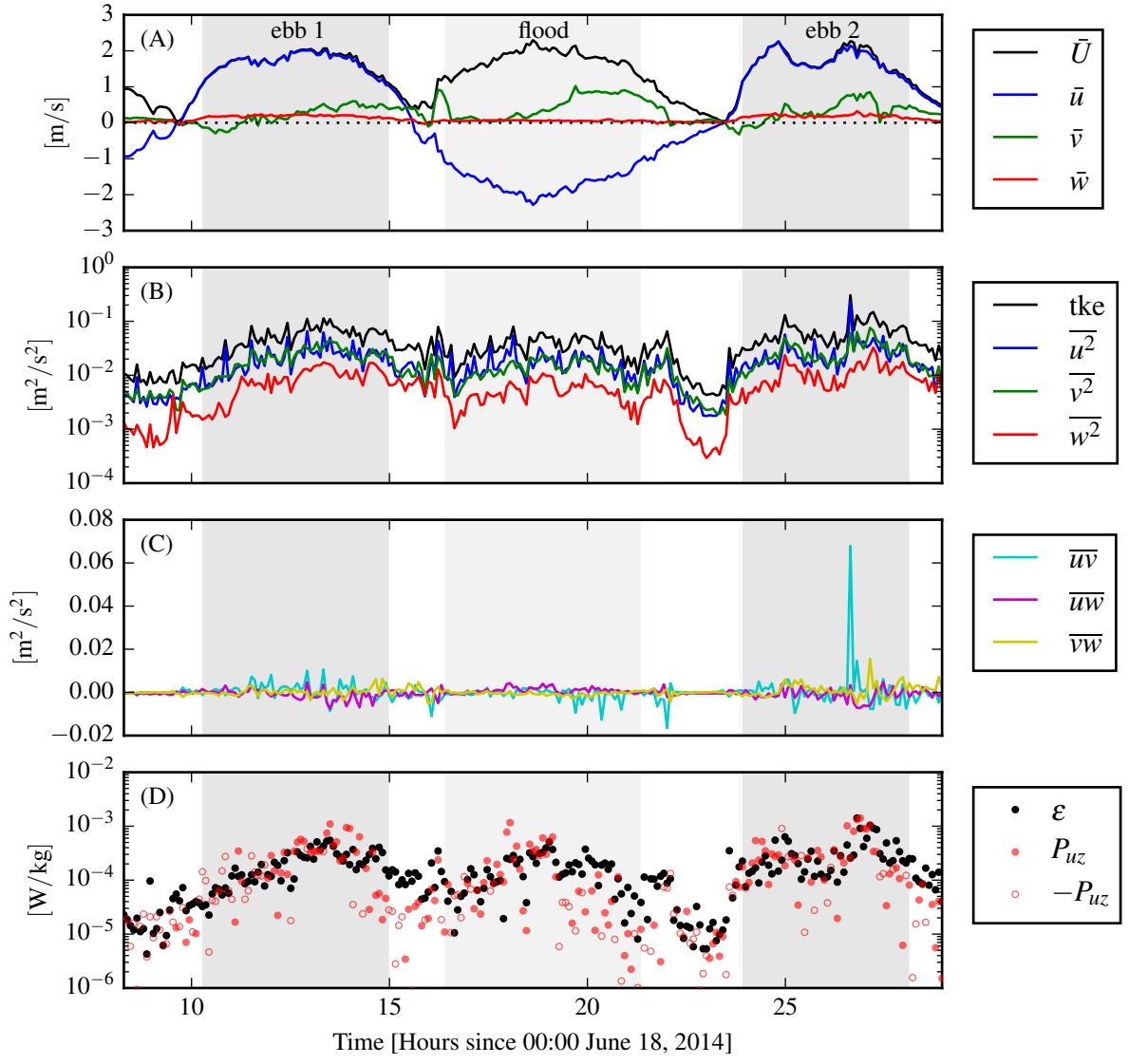

FIG. 11. Time-series of mean velocities (A), turbulence energy and its components (B), Reynold's stresses (C), and turbulence dissipation rate (D) measured by the TTM during the June, 2014 deployment. Shading indicates periods of ebb ($\bar{u} > 1.0$, grey), and flood ($\bar{u} < -1.0$, lighter grey).

(C), dissipation and one component of turbulence production (D) grow and strengthen with ebb or flood, then subside during slack tide. This component of turbulence production is:

$$P_{uz} = \frac{\partial \bar{u}}{\partial z}\overline{uw} \quad . \tag{5}$$

Where $\partial\bar{u}/\partial z$ is computed from the $\bar{u}$ measurements from the two ADV's on the TTM, which are separated vertically by 0.5 m. The highest values of ε and P_{uz} occur in the middle of the ebb or flood, which is in agreement with other measurements in tidal channels. The agreement of the magnitude of the P_{uz} with ε at those times suggests a local production-dissipation balance that is often observed in tidally forced channels (Trowbridge et al. 1999; Stacey et al. 1999; McMillan et al. 2016). At other times the value of P_{uz} is insufficient to balance ε or is negative.

Inspection of the negative P_{uz} values reveals that the vast majority of them are due to a reversed sign of $\overline{uw}$, rather than a reversed sign of $\partial u/\partial z$. This suggests that uncertainty in $\overline{uw}$ may be contributing to discrepancies between P_{uz} and ε. It is also possible that other terms of the tke equation are important, such as other components of production, advection terms, or turbulent transport terms.

Figure 12 compares individual values of P_{uz} with ε directly. Given the assumptions implicit in this comparison,

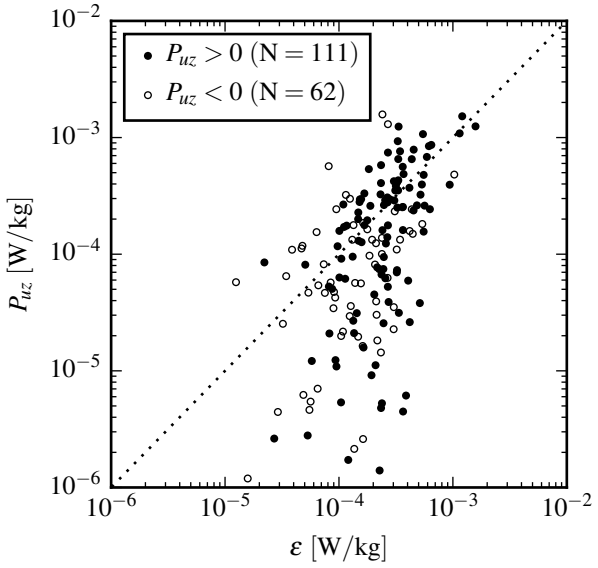

FIG. 12. P_{uz} vs. ε during the June 2014 TTM deployment. Values of 'negative' production are indicated as open circles.

and the discussion above, the agreement between P_{uz} and ε is an encouraging result that suggests the turbulent boundary reaches the depth of these measurements (10 m) during the highest flow speeds. This results is further supported by a comparison of $\bar{U}$ with ε (Figure **??**). Here we see a $\varepsilon \propto \bar{U}^3$ dependence that is again suggestive of bottom boundary layer physics Trowbridge (1992); Nash et al. (2009). At lower flow speeds, ε deviates from this relationship, which suggests that the boundary layer is no longer the dominant physical process at the depth of these measurements.

6. Conclusion

Acknowledgments. Many thanks to Joe Talbert, Alex DeKlerk, Captain Andy Reay-Ellers, Maricarmen Guerra, Marshall Richmond, James VanZwieten, Matthew Egeland and Jennifer Rinker.

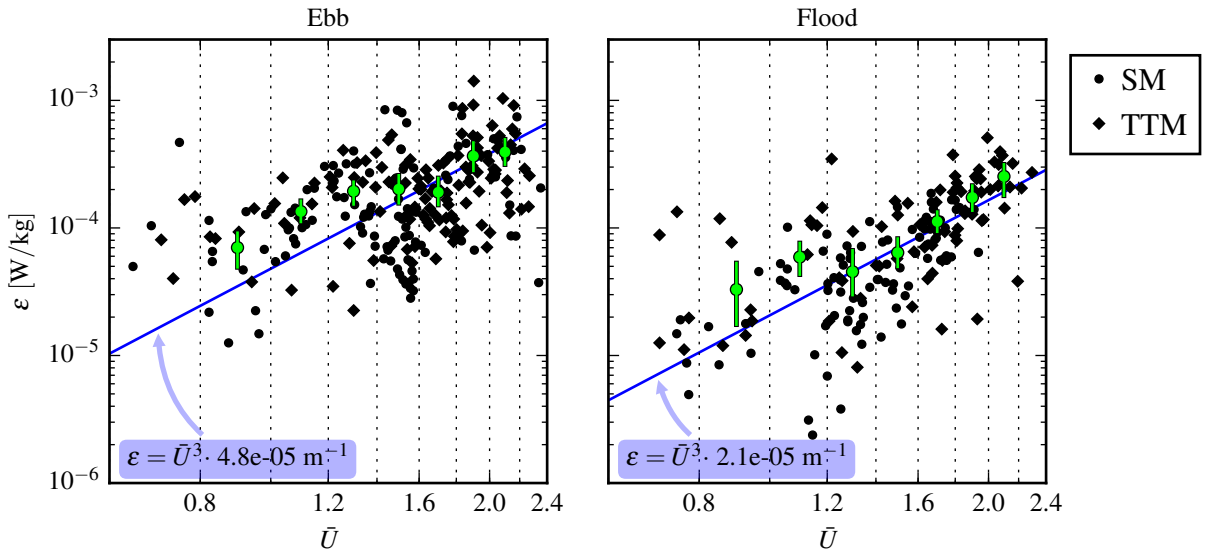

FIG. 13. A log-log plot of ε versus $\bar{U}$ for the June 2014 TTM (diamonds) and May 2015 StableMoor (dots) deployments, during ebb (left) and flood (right). Black points are 5 minute averages. Green dots are mean values within speed bins of 0.2 m s^{-1} width that have at least 10 points (50 minutes of data); their vertical bars are 95% bootstrap confidence intervals. The blue line shows a U^3 slope, where the proportionality constant (blue box) is calculated by taking the log-space mean of ε/U^3.

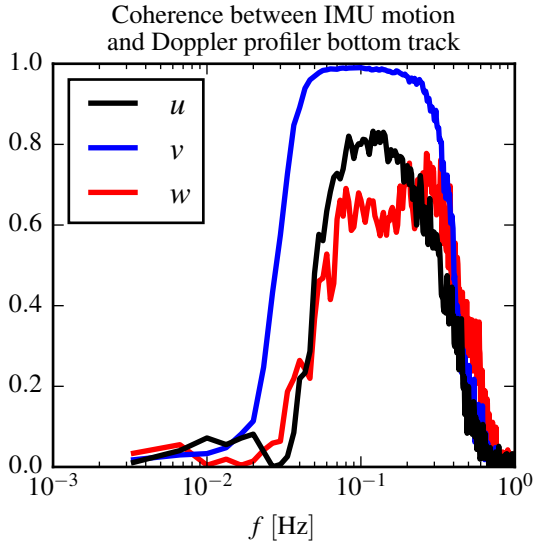

FIG. A1. Coherence between stablemoor IMU measured motion and bottom track velocity.

APPENDIX

A1. Comparing StableMoor $\vec{u}_{\text{low}}$ to IMU $\vec{u}_{\text{h}}$

It is instructive to compute compare the motion of the StableMoor buoy as measured by the Compare the motion correction of SM to TTM: SM does better because it is more stable, and has a measurement of u_{low}. Discuss spectral coherence of u_{BT} with IMU, i.e. Figure A1. This is important because it shows the low-f limit of the IMU measured motion.

References

Barshan, B., and H. F. Durrant-Whyte, 1995: Inertial navigation systems for mobile robots. *IEEE Transactions on Robotics and Automation*, **11 (3)**, 328–342.

Bevly, D. M., 2004: Global positioning system (gps): A low-cost velocity sensor for correcting inertial sensor errors on ground vehicles. *Journal of dynamic systems, measurement, and control*, **126 (2)**, 255–264.

Egeland, M. N., 2014: Spectral evaluation of motion compensated ADV systems for ocean turbulence measurements. Ph.D. thesis, Florida Atlantic University.

Grant, H. L., R. W. Stewart, and A. Moilliet, 1962: Turbulence spectra from a tidal channel. *Journal of Fluid Mechanics*, **12**, 241–263.

Gulmammadov, F., 2009: Analysis, modeling and compensation of bias drift in mems inertial sensors. *Recent Advances in Space Technologies, 2009. RAST'09. 4th International Conference on*, IEEE, 591–596.

Harding, S., L. Kilcher, and J. Thomson, 2016: Motion of tethered instrument platforms for acoustic doppler velocimetry in energetic tidal flows, simul-pub?

Kilcher, L., J. Thomson, J. Talbert, and A. DeKlerk, 2016: Measuring turbulence from moored acoustic Doppler velocimeters: A manual to quantifying inflow at tidal energy sites. Tech. Rep. 62979, National Renewable Energy Laboratory. URL www.nrel.gov/docs/fy16osti/62979.pdf.

Kolmogorov, A. N., 1941: Dissipation of energy in the locally isotropic turbulence. *Dokl. Akad. Nauk SSSR*, **32 (1)**, 16–18, URL http://www.jstor.org/stable/51981.

Lumley, J., and E. Terray, 1983: Kinematics of turbulence convected by a random wave field. *Journal of Physical Oceanography*, **13 (11)**, 2000–2007.

McMillan, J. M., A. E. Hay, R. G. Lueck, and F. Wolk, 2016: Rates of dissipation of turbulent kinetic energy in a high reynolds number tidal channel. *Journal of Atmospheric and Oceanic Technology*, **33 (4)**, 817–837, doi:10.1175/JTECH-D-15-0167.1, URL http://dx.doi.org/10.1175/JTECH-D-15-0167.1, http://dx.doi.org/10.1175/JTECH-D-15-0167.1.

MicroStrain, I., 2010: Technical note: Coning and sculling. Tech. Rep. I0019, MicroStrain. URL http://files.microstrain.com/TN-I0019_3DM-GX3-25_-Coning_And_Sculling.pdf.

Morison, J. R., J. W. Johnson, and S. A. Schaaf, 1950: The force exerted by surface waves on piles. *Journal of Petroleum Technology*, **2 (05)**, 149–154.

Nash, J. D., L. F. Kilcher, and J. N. Moum, 2009: Structure and composition of a strongly stratified, tidally pulsed river plume. *Journal of Geophysical Research*, **114**, C00B12, doi:10.1029/2008JC005036.

Sreenivasan, K. R., 1995: On the universality of the Kolmogorov constant. *Physics of Fluids*, **7**, 2778–2784.

Stacey, M. T., S. G. Monismith, and J. R. Burau, 1999: Observations of turbulence in a partially stratified estuary. *Journal of Physical Oceanography*, **29**, 1950–1970.

Thomson, J., B. Polagye, V. Durgesh, and M. Richmond, 2012: Measurements of turbulence at two tidal energy sites in Puget Sound, WA. *Journal of Oceanic Engineering*, **37 (3)**, 363–374, doi:10.1109/JOE.2012.2191656.

Trowbridge, J. H., 1992: A simple description of the deepening and structure of a stably stratified flow driven by a surface stress. *Journal of Geophysical Research*, **97**, 15 529–15 543.

Trowbridge, J. H., W. R. Geyer, M. M. Bowen, and A. J. I. Williams, 1999: Near-bottom turbulence measurements in a partially mixed estuary: turbulent energy balance, velocity structure and along-channel momentum balance. *Journal of Physical Oceanography*, **29**, 3056–3072.

van der Walt, S., S. C. Colbert, and G. Varoquaux, 2011: The numpy array: A structure for efficient numerical computation. *Computing in Science & Engineering*, **13**, 22–30, doi:10.1109/MCSE.2011.37, URL http://scitation.aip.org/content/aip/journal/cise/13/2/10.1109/MCSE.2011.37.

Walter, R. K., N. J. Nidzieko, and S. G. Monismith, 2011: Similarity scaling of turbulence spectra and cospectra in a shallow tidal flow. *Journal of Geophysical Research: Oceans*, **116 (C10)**.